The Journal of Chemical Physics

Detection of single DNA mismatches by force spectroscopy in short DNA hairpins

Cite as: J. Chem. Phys. **152**, 074204 (2020); https://doi.org/10.1063/1.5139284
Submitted: 19 November 2019 . Accepted: 02 February 2020 . Published Online: 19 February 2020

F. Landuzzi, X. Viader-Godoy, F. Cleri, I. Pastor, and F. Ritort

The Journal of Chemical Physics ARTICLE scitation.org/journal/jcp

Detection of single DNA mismatches by force spectroscopy in short DNA hairpins

Cite as: J. Chem. Phys. 152, 074204 (2020); doi: 10.1063/1.5139284
Submitted: 19 November 2019 • Accepted: 2 February 2020 •
Published Online: 19 February 2020

F. Landuzzi,[1,2,a)] X. Viader-Godoy,[3] F. Cleri,[2,4] I. Pastor,[3,5] and F. Ritort[3,5,b)]

AFFILIATIONS

[1] Department of Physics, Aoyama Gakuin University, 5-10-1 Fuchinobe, Chuo-ku, Sagamihara, Japan
[2] I.E.M.N. (UMR Cnrs 8520), 59652 Villeneuve d'Ascq, France
[3] Small Biosystems Lab., Univ. de Barcelona, Diagonal 647, 08028 Barcelona, Spain
[4] Département de Physique, Université de Lille, 59650 Villeneuve d'Ascq, France
[5] CIBER-BBN de Bioing., Bioma. y Nanomed., Inst. de Sanidad Carlos III, Madrid, Spain

[a)] **Electronic mail:** landuzzi.fabio@gmail.com
[b)] **Author to whom correspondence should be addressed:** fritort@gmail.com

ABSTRACT

Identification of defective DNA structures is a difficult task, since small differences in base-pair bonding are hidden in the local structural variability of a generally random base-pair sequence. Defects, such as base mismatches, missing bases, crosslinks, and so on, occur in DNA with high frequency and must be efficiently identified and repaired to avoid dire consequences such as genetic mutations. Here, we focus on the detection of base mismatches, which is local deviations from the ideal Watson–Crick pairing rule, which may typically originate from DNA replication process, foreign chemical attack, or ionizing radiation. Experimental detection of a mismatch defect demands the ability to measure slight deviations in the free energy and molecular structure. We introduce different mismatches in short DNA hairpins (10 or 20 base pairs plus a 4-base loop) sandwiched between dsDNA handles to be used in single-molecule force spectroscopy with optical tweezers. We perform both hopping and force-pulling experiments to measure the excess free energies and deduce the characteristic kinetic signatures of the mismatch from the force–distance curves. All-atom molecular dynamics simulations lend support to the detailed interpretation of the experimental data. Such measurements, at the lowest sensitivity limits of this experimental technique, demonstrate the capability of identifying the presence of mismatches in a random complementary dsDNA sequence and provide lower bounds for the ability to distinguish different structural defects.

INTRODUCTION

A DNA mismatch (MM) is a structural defect occurring when two non-complementary bases are aligned in a sequence of duplex DNA.[1] An MM is defined as *transduction* when formed by non-complementary purine–pyrimidine (pur–pyr) bases and *transversion* in the case of pur–pur or pyr–pyr pairs. Compared to DNA strands with the canonical (Watson–Crick) pairing rules, MMs are expected to produce alterations in the structure and stability of the DNA helix, especially in the proximity of the MM site.[2–4] MMs can appear during replication of DNA,[5] heteroduplex formation,[6] as well as by action of mutagenic chemicals, ionizing radiation, or spontaneous deamination.[7] MMs are efficiently corrected in DNA by mismatch repair (MMR) proteins.

Failures in detecting or correcting the lesion give rise to genetic mutations;[7,8] in fact, MMs have been associated with 10%–30% of spontaneous cancers in various tissues.[8,9] In particular, G-A and G-T defects are of great interest to the cancer biology community, since such a type of MM can be formed efficiently during oxidative stress, both by endogenous processes and following chemo- or radiotherapy. A prominent example is the so-called 8-oxoG lesion,[10] which differs from ordinary guanine in that an H atom is replaced by an O atom at the C8 position and the N7 nitrogen becomes protonated. Such defects can be formed by several reactive oxygen species (ROS) that are able to attack guanine. In the subsequent replication

stage, 8-oxoG displays a higher affinity for adenine than cytosine, thereby leading to a 8-oxoG-A mismatch and, ultimately, to a G-C → T-A mutation. Another common mismatch is the G-T formed with high probability by polymerases such as β and Taq, during DNA replication, thus being about a thousand fold more frequent than other MMs; this is mainly due to its strong thermodynamic stability, which makes its identification by repair enzymes quite difficult.[11]

Powerful approaches are available to detect specific locations of DNA sequence variation, such as rolling circle amplification,[12] molecular inversion probes,[13] and MM ligation with bioluminescence detection,[14] all based on DNA ligase or nuclease activities; Taqman probes, molecular beacons, and related assays have also been used to detect specific targeted alleles.[15,16] All of these methods require *a priori* knowledge of the reference sequence and involve the construction of sophisticated probes. By contrast, MM-detection assays rely on the base-pairing quality of DNA, and subsequent enzymatic detection of mispaired bases,[17,18] and are thus independent of the exact identity of the underlying mutation. All such methods are suitable for high-throughput screening of unknown sequences and work on large populations of identical DNA sequences properly amplified by molecular engineering techniques. On the other hand, the detailed molecular structure modifications of individual DNA defects have been assessed by nuclear magnetic resonance (NMR) and x-ray diffraction,[19–22] most notably for the typical G-T mismatch. However, the thermodynamic and kinetic changes in the stability of the DNA structure induced by such defects remain inaccessible to such techniques. Such details are indeed crucial to understand the extremely selective ability of repair enzymes (glycosylases), which are capable of rapidly scanning the DNA sequence at rates of 20–30 bp/s[23] while applying small forces to the backbone in a sort of highly dynamical "interrogation" process aimed at detecting differences of just a few kcal/mol.[24]

In recent years, many efforts have been devoted to experimentally characterize the biomolecular free-energy landscape of folding.[25] Dynamic force spectroscopy experiments are well-suited to study the folding/unfolding transitions of one molecule at a time with high spatial and temporal resolution.[26–28] From the experimentally measured force-dependent unfolding and folding kinetic rates, it is possible to characterize the position of the transition states and the height of the corresponding kinetic barriers.[29] Notably, force spectroscopy by laser optical tweezers (LOT) has been successfully applied to measure short DNA hairpin sequences, thereby allowing us to detect the elastic properties of ssDNA,[30] and transition states during the repeated folding/unfolding pullings.[31] In a recent study,[32] LOT were used to characterize four different MMs, by positioning pairs of identical defects at a close distance in 29-bp DNA hairpins with a 6-base loop. AFM-based force spectroscopy studies have demonstrated the possibility of detecting single DNA mismatches by measuring irreversible rupture force distributions in oligonucleotide microarrays[33] and DNA origami platforms.[34] However, the question remains whether mismatch free energy differences in a DNA duplex can be determined in pulling assays.

In this work, we use force spectroscopy with LOT to demonstrate the capability to measure the excess free energy of individual MMs in DNA at the single molecule level. To this end, we have synthesized very short DNA hairpins, of 10 and 20 bp stem length, containing single G-A or G-T mismatches. Hairpins are tethered between two double-stranded (ds) DNA handles of 29 bp each. We investigated two different stem lengths to ensure sufficiently high signal-to-noise ratio measurements to derive the excess free energy in all constructs. We find that the identification of single mismatches in pulling assays is facilitated using different protocols depending on the length of the hairpin. While for hairpins shorter than 10–20bp, equilibrium hopping experiments are more convenient, above 20bp, nonequilibrium pulling experiments give a better signal. The study of two constructs with two different protocols (hopping vs pulling) allows us to monitor the internal dynamics of the native (i.e., the canonical hairpin with the Watson–Crick bp only) and defective molecules. It also permits us to test the robustness of the measured excess energy values. Our results demonstrate the ability of the method to clearly detect the presence of single MM defects in the DNA sequence; defect energetics and dynamics can be qualitatively and quantitatively characterized within the lower limits of the experimental resolution. A set of Molecular Dynamics (MD) simulations supports the interpretation of the experimental data and provides useful indications about the molecular details of the unfolding process over a finer time scale that escapes the experimental resolution. The experimental method combined with numerical simulations offers a promising route to the characterization of defects in DNA sequences and their interaction with damage-signaling and repair proteins.

MATERIALS AND METHODS

Optical tweezers setup and DNA substrates

The experiments are carried out using a miniaturized dual-beam setup LOT described in the work of Huguet *et al.*[35] Briefly, two counter-propagating laser beams (P = 200 mW and λ = 845 nm) are tightly focused, creating a single optical trap. Experiments are performed by tethering a DNA molecule between two polystyrene beads, one is held by air suction at the tip of a glass pipette and the other is captured in the optical trap and used to measure the force by measuring the deflection light with position sensing detectors (PSDs). Figure 1(a) shows a schematic representation of the experimental setup. Tethers are made by ssDNA tails that are labeled with one biotin (oligos acquired this way) or several digoxigenins (see the supplementary material for detailed information), which can bind selectively to streptavidin- (2.1 μm Kisker Biotech) or anti-digoxigenin-coated beads (3.0–3.4 μm Kisker Biotech), respectively. The position of the optical trap is determined by diverting ≈8% of each laser beam to a secondary PSD. The instrument has a resolution of 0.1 pN and 1 nm at a 1 kHz acquisition rate.

The DNA constructs studied in this work consist of a dsDNA segment (called stem) of either 10 or 20bp inserted between two 29bp segments called handles. The two strands of the stem are connected via a loop of 4 bases. The sequences of the stem and loop region are shown in Figs. 1(b) and 1(d). Each handle is tailed either with biotin or digoxigenin in order to attach it specifically to streptavidin- or antidigoxigenin-coated beads. The synthesis of the hairpins is described in detail in the supplementary material. Shortly, an oligo with the stem sequence (10 or 20bp), sided by

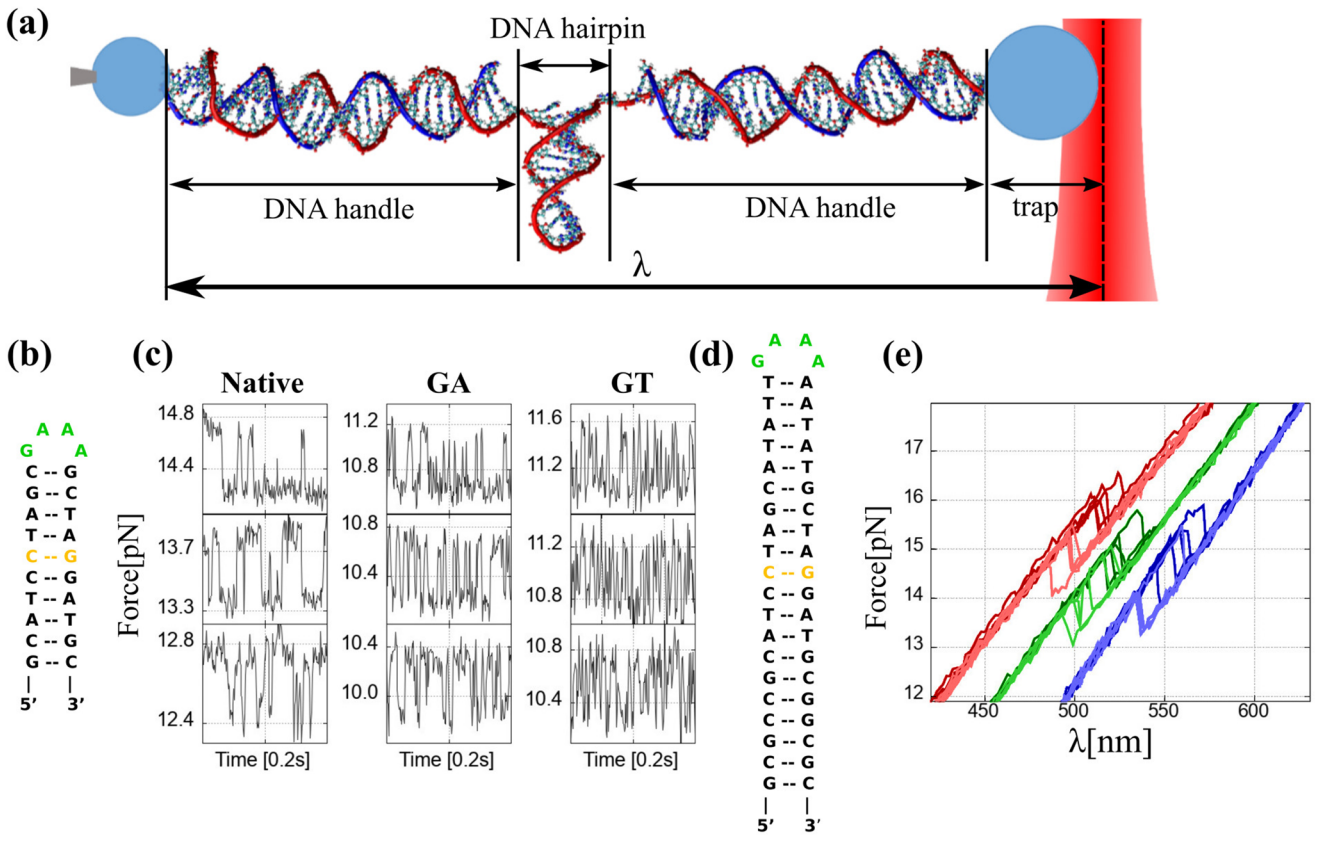

FIG. 1. Experimental setup and DNA sequences. (a) Schematic representation of the LOT experimental setup. A DNA hairpin is attached between two micron-sized beads via dsDNA handles. One bead is held by air suction at the tip of a glass micropipette, while the other is captured in the optical trap. λ is the distance between the tip of the pipette and the center of the optical trap. (b) Sequence of the 10bp hairpins with the 4-loop (green) and the single mismatch location (yellow). (c) Experimental force–time traces for the 10pb hairpin hopping experiments.(d) Sequence of the 20bp hairpins with the 4-loop (green) and the single mismatch location (yellow). (e) Several FDC cycles for native (red), G-A mismatch (green), and G-T mismatch (blue) 20bp hairpins. In dark (light) colors are shown the stretching (releasing) curves.

29b (corresponding to the handles) on each side (Sigma-Aldrich), is digoxigenin-tailed and annealed to the handle-region complementary 29b oligo. All our experiments are performed in TE buffer (Tris 10 mM and 1 mM EDTA) pH 7.5M, 1M NaCl at room temperature (298 K).

Hopping experiments

In hopping experiments, the pipette and optical trap relative distance, λ, is kept fixed, while the hairpin executes transitions between the folded and unfolded states. An example of experimental force-traces for hopping experiments is shown in Fig. 1(c). We monitored the force at 1 kHz for 15–40 s, for a time sufficient to register at least 20 conformational transition events and then slightly moved the distance λ and repeated the measurement. Notably, once λ is fixed, the force in the unfolded state is lower than that in the folded state because the bead experiences a much larger displacement from the center of the optical trap when the hairpin is formed. As a consequence, if such a force jump between the two states is larger than the thermal noise, monitoring the instantaneous force is equivalent to collecting information on the state (folded vs unfolded) of the hairpin. By working in the vicinity of f_c, at which the two states have the same occupation probability, the kinetic rates of unfolding (k^+) and folding (k^-) fall in a time scale that allows us to observe several hopping events. Each variation of the trap position, λ, produces a consequent variation of the probability to observe the system in the folded (w_N) or unfolded (w_U) state. Upon repeating the measurements at different λ's, we could measure the relative variation of the occupation probability of the two states. Typical time-series and probability histogram data for 10bp hairpins, with a native sequence or including a GA and GT mismatch, are presented in Fig. 2(a), and Figs. 3–5 of the supplementary material.

Pulling experiments

In a ramping protocol, the trap position is moved at a constant speed while force is measured. Typical force–distance curves (FDC) are shown in Fig. 1(e) (a more detailed plot for the mismatch GA, GT, and different pulling velocities are reported in Figs. 6–9 of the supplementary material). At low forces, hairpins are in the

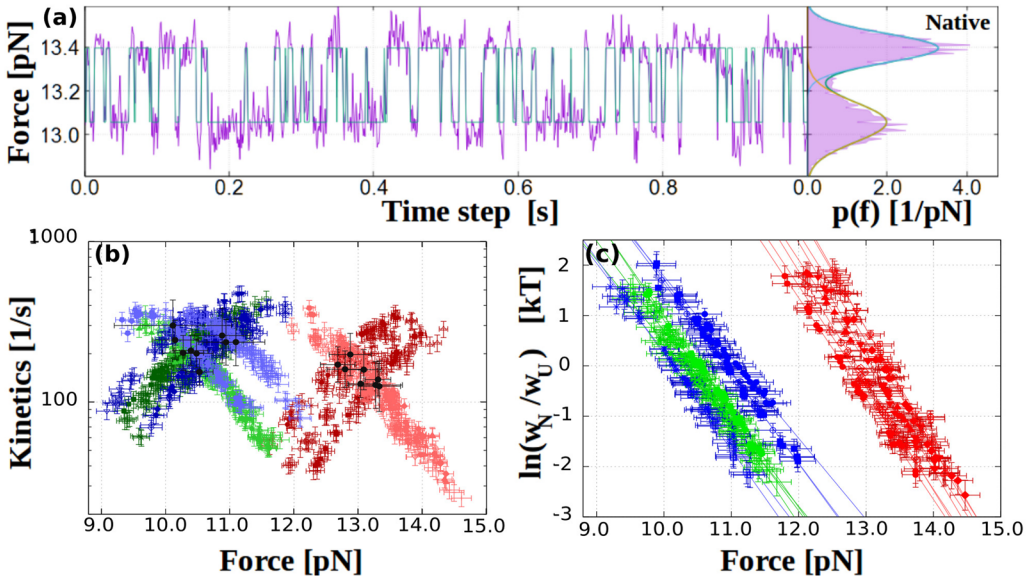

FIG. 2. 10bp hairpin hopping results. (a) Example of a hopping trace of the 10bp native hairpin (left panel), the green curve is the optimal trajectory obtained from the HMM. Force distributions (right panel) together with the best-fit from the HHM (blue curve) and the two-state Gaussian fit from Eq. (2) (green and yellow curves for each Gaussian component). (b) Unfolding (dark color) and refolding (light color) kinetic rates measured for the native (red), G-A mismatch (green), and G-T mismatch (blue) hairpins. The validity of the BE approximation is shown as a straight line in the semi-log scale. (c) Plot of $\ln(w_N/w_U)$ as a function of force from Eq. (3) for the three hairpins. Color code as in (b).

folded state, with the stem forming a double helix; whereas at large forces, they unfold to a stretched conformation, where the stem is found as ssDNA.[36] Transitions between both states are viewed in the FDC as a sudden jump in force. Forces at which such transitions take place change upon repeating the same experiment due to thermal fluctuations. Typically, two force branches are observed: the upper force branch shows the elastic response of the whole molecular construct when the hairpin is folded, whereas the lower force branch shows the response for the unfolded hairpin. By analyzing the folding/unfolding trajectories, it is possible to detect the force value at which the hairpin unfolds/refolds for the first time along the trajectory; this is called the first-rupture force and appears [see Fig. 1(d), and Figs. 6–10 of the supplementary material] as a force rip along the FDC. For the 10bp hairpins, the rupture force distribution is not clearly detectable since the kinetic rates are comparable with the recording data frequency and the force fluctuations are comparable to the force jump, as shown in the trajectories in Fig. 10 of the supplementary material. For this reason, only the 20bp hairpin pulling data (shown in Figs. 6–8 of the supplementary material), have been used in this work. For each sequence (native and GA and GT mismatches), we averaged measurements on at least three molecules at 100 nm/s. Force-pulling experiments typically covered 50–100 cycles.

Kinetic rate theory

Information about the molecular free energy landscape (mFEL) can be obtained by analyzing the data using kinetic models, such as the Bell–Evans (BE) model.[37,38] The BE model predicts an exponential dependence on force of the folding and unfolding kinetic rates,

$$\begin{aligned} k^{+}(f) &= k_0 \exp[-\beta(B_{TS} - f \cdot x_{N\to TS})] \\ &= k_m \exp[\beta f \cdot x_{N\to TS}], \\ k^{-}(f) &= k_0 \exp[-\beta(B_{TS} - \Delta G_{NU} + f \cdot x_{TS\to U})] \\ &= k_m \exp[-\beta(f \cdot x_{TS\to U} - \Delta G_{NU})], \end{aligned} \tag{1}$$

where ΔG_{NU} is the free-energy difference between N and U extrapolated to zero force and $x_{N\to TS}$ ($x_{U\to TS}$) are the distances between the x_{TS} and the folded (unfolded) state that are taken as force independent. B_{TS} is the kinetic barrier extrapolated to zero force and has been included in the prefactor $k_m = k_0 \exp(-\beta B_{TS})$. At the coexistence force f_c, $k^{+}(f_c) = k^{-}(f_c)$, and therefore, $\Delta G_{NU} = f_c(x_{N\to TS} + x_{TS\to U}) = f_c x_{NU}$ with x_{NU} being the released molecular extension at f_c. Bell–Evans kinetic rates are a valid approximation close to f_c, and deviations are expected at sufficiently low or high forces.[39] From these phenomenological equations, we could fit the kinetic rates obtained by the analysis of the pulling and hopping data with the force and extract the free-energy of formation, the molecular extension, and the kinetic rate at the coexistence force. The BE approximation is valid in a small range of forces not too far from the coexistence force, f_c.

Molecular dynamics simulations

For the molecular dynamics (MD) simulations, we used the GROMACS 5.1 computer code.[40,41] The hairpin plus handles

molecular construct [see Fig. 1(a)] was built as a continuous ssDNA chain spanning from the 5′ to the 3′ ends: the first and last groups of 29 bases were matched to two complementary 29-long ssDNA strands, to make up the two dsDNA handles; the central 10 + 4 + 10 bases represented the hairpin, perfectly folded in the initial configuration. The end-to-end distance between the C1′ atoms of the first and last bp (to be used as the reference length hereafter) is $\lambda_0 = 23$ nm. The structure of hairpin plus handles, with the same native base sequence used in the experiments, was assembled in a water box of size $50 \times 9 \times 12$ nm^3 with periodic boundary conditions in the three directions, containing about 174 000 TIP3P water molecules, plus 625 Na^+ and 488 Cl^- ions, to ensure neutralization of the phosphate backbone charge, and physiological salt concentration around 0.15M.

Equilibrium MD simulations were carried out at temperatures ranging from 300 K to 360 K and a pressure of 1 atm at constant-{*NVT*}. Coulomb forces were summed by shifted particle-mesh Ewald electrostatics, with real space cutoff set at 1 nm; long-range dispersion forces were also cut off at 1 nm. We used rigid bonds for the water molecules, which allowed us to push the time step to 1 fs for both the thermal equilibration runs and the force-pulling simulations. Typical preparatory constant-{*NPT*} MD runs lasted between 10 ns and 20 ns; force-pulling simulations were carried out for 50 ns; thermal equilibrium simulations at constant-{*NVT*} lasted typically 100 ns.

Steered molecular dynamics (SMD) were performed on the fragments with the constant-force pull code available in GROMACS. We applied a constant displacement/force parallel to the direction x by means of a harmonic-spring fictitious potential attached to the center of mass of the last base pair of the DNA handles. After some tests, the spring constants were set at 100 kJ mol^{-1} nm^{-2} and 75 kJ mol^{-1} nm^{-2}, which is ~1000 times higher than typical values of experiments performed with OT. Pulling speeds of about 20 cm/s were used for most SMD simulations. Forces and displacements were recorded at intervals of 10 time steps.

We also consider the possibility to study this system using a coarse-grained model.[42,43] We have performed simulation tests using the oxDNA2 model with sequence dependent stacking interaction implemented in LAMMPS.[44] This model has been used by other researchers to estimate the FEL of a short hairpin in melting.[45] Despite the increased simulation time (anyway not sufficient to obtain a proper kinetics characterization), these models have been tested only for the native sequence and do not account for relevant structural differences between purine and pyrimidine for mismatched base pairs. Moreover, the implicit solvent does not completely account for the hydrodynamic effects during the pulling protocol. It is for these reasons that we decide to focus on the all-atom model.

RESULTS

Free energy measurements from hopping experiments in 10bp DNA hairpins

Figure 2(a) (left) shows an example of an experimental hopping trace for the 10 bp native hairpin, while Fig. 2(a) (right) shows the histogram of the force distribution that can be well fitted to a sum of two Gaussians,

$$P_\lambda(f) = \frac{w_{\lambda,U}}{\sqrt{2\pi\sigma^2_{\lambda,U}}} e^{-\left(\frac{f-\langle f_{\lambda,U}\rangle}{4\sigma_{\lambda,U}}\right)^2} + \frac{w_{\lambda,N}}{\sqrt{2\pi\sigma^2_{\lambda,N}}} e^{-\left(\frac{f-\langle f_{\lambda,N}\rangle}{4\sigma_{\lambda,N}}\right)^2}, \quad (2)$$

where $\langle f_{\lambda,U}\rangle$, $\langle f_{\lambda,N}\rangle$ represent the average force in the unfolded and folded state, respectively, and $\sigma_{\lambda,U}$, $\sigma_{\lambda,N}$ are the standard deviations of the force. A more accurate statistical analysis of the hopping traces based on hidden Markov models reveals only two underlying molecular conformations N and U (see the Hidden Markov model section of the supplementary material).

It must be noted that, for any fixed value of λ, the two kinetic rates in Eq. (1) are evaluated at different force values, namely, $k^+(f)$ ($k^-(f)$) is measured at force f_N (f_U) where the molecule hops from N to U (U to N). Therefore, we can separately plot $k^+(f_N)$ and $k^-(f_U)$, with λ acting as a parameter. These rates measured in the passive mode, where the force is not kept constant, are called apparent rates.[46] These data, plotted in Fig. 2(b), mark two important points: first, for each type of hairpin, the coexistence force, f_c, is readily identified by the value at which $k^+ = k^-$; second, the exponential dependence of the rates on the force indicates that the BE model[37,47] should be applicable in this case.

Moreover, the molecule is found to follow exponential kinetics.[29] The probability distribution of the residence times in the folded/unfolded conformations is well described by an exponential function whose width is equal to the inverse of the unfolding/folding kinetic rate. The dependence of these rates on the applied force provides accurate information about the height and position of the kinetic barrier.

From Eq. (1), we can express the ratio between the kinetic rates in the form

$$\begin{aligned} k_B T \log\left(\frac{k^+(f)}{k^-(f)}\right) &= k_B T \log\left(\frac{w_U(f)}{w_N(f)}\right) \\ &= -\Delta G_{NU} + f \cdot (x_{N\to TS} + x_{TS\to U}) \\ &= (f - f_c) \cdot x_{NU}, \end{aligned} \quad (3)$$

with $\Delta G_{NU} = f_c x_{NU}$ being the free energy difference extrapolated to zero force. Figure 2(c) shows the $\ln(w_N/w_U)$ vs force for all the 10-bp hairpins studied.

We can also estimate the free energy between N and U at zero force using the following formula (see the supplementary material for more details):

$$\Delta G^0_{NU} = \int_0^{f_c} x_{ssDNA}(f')df' - \int_0^{f_c} x_d(f')df', \quad (4)$$

where f_c is defined by $k^+(f) = k^+(f)$ or $w_N(f_c) = w_U(f_c)$ [see Eq. (3)]. While the estimation $\Delta G_{NU} = f_c x_{NU}$ in Eq. (3) is an extrapolated value using the BE model, Eq. (4) is an exact thermodynamic relation for ΔG_{NU}, which, however, requires accurate knowledge of the elastic response of ssDNA and the hairpin diameter.

Table I shows the experimental parameters obtained using the BE model and the theoretical ones predicted by the unified oligonucleotide thermodynamic dataset incorporating mismatches.[3] The theoretical predictions of the FEL are obtained using the mfold Web Server[48] and take into account the contribution coming from the tetraloop (see Fig. 2 of the supplementary material). It is worth noting that the values of ΔG_{NU} and ΔG^0_{NU} [Eqs. (3) and (4)] are compatible with each other. However, the theoretically predicted value of

TABLE I. 10bp results. Parameters obtained from the hopping experiments for the 10 bp hairpins from the Bell–Evans model and compared with the theoretical values obtained from the nearest-neighbor model[3] with the contribution of the tetraloop (see Fig. 2 of the supplementary material). The theoretical f_c is obtained from Eq. (3) imposing $\Delta G_{NU}(f_c) = 0$.

Hairpin	f_c (pN)	x_{NU} (nm)	$x_{N\to TS}$ (nm)	$x_{TS\to U}$ (nm)	ΔG_{NU} (k_BT)	ΔG^0_{NU} (k_BT)
10bp native	13.0 ± 0.4	8.7 ± 0.5	4.1 ± 0.4	4.6 ± 0.3	27 ± 4	21 ± 2
Theor. native	14.7	8.8	/	/	24.2	
10bp GA	10.4 ± 0.3	7.1 ± 0.7	3.4 ± 0.2	3.8 ± 0.6	18 ± 2	16 ± 2
Theor. GA	11.8	8.4	/	/	18.1	
10bp GT	10.6 ± 0.6	6.1 ± 0.5	3.0 ± 0.5	3.1 ± 0.4	16 ± 3	16 ± 2
Theor. GT	11.6	8.5	/	/	17.6	

f_c overestimates the experimental result by ≃1.5 pN. In addition, the theoretical and experimental values of x_{NU} agree for the native hairpin, while for the hairpins with mismatches, the experimental value is underestimated by 1–2nm.

Free energy measurements from pulling experiments in 20bp DNA hairpins

Figure 3 shows the results of pulling experiments. From the FDCs [Fig. 3(a)], we extract the rupture force distributions $\rho_{N(U)}(f)$ and survival probabilities $P_{N(U)}(f)$, which are related by $\rho_{N(U)}(f) = -P'_{N(U)}(f)$. Kinetic rates can be extracted from the rate equations

$$\frac{dP_N(f)}{df} = -\frac{k^+(f)}{r}P_N(f) \Rightarrow k^+(f) = \frac{r\rho_N(f)}{P_N(f)},$$
$$\frac{dP_U(f)}{df} = -\frac{k^-(f)}{r}P_U(f) \Rightarrow k^-(f) = \frac{r\rho_U(f)}{P_U(f)}, \quad (5)$$

with $r = k_{\text{eff}}v_{\text{pull}}$ being the loading rate and k_{eff} being the effective stiffness (equal to the slope of the FDC).

Figure 3(b) shows the results for the kinetic rates vs force in semi-log scale obtained from Eq. (5) and fitted to exponential functions as predicted by the BE model [Eq. (1)]. The coexistence force is shown as the crossing point of the fits [black points in Fig. 3(b)]. From the fitting parameters and using Eq. (3), we extract ΔG_{NU}. The results are shown in Table II.

Simulation results

We realized a series of molecular dynamics (MD) simulations on the 10bp hairpin with the native sequence, as described in the Materials and methods section. Given the extremely large difference between the experimental and MD time scales, a direct comparison between the theoretical and experimental results is not possible, notably as far as estimates of defect energies are concerned. Therefore, we focused the simulations only on the native hairpin sequence, aiming to provide additional insight into the molecular-scale phenomena that could be relevant to analyze and interpret the experimental results.

In a first type of *non-equilibrium* MD simulations, we performed simulated force-pulling experiments on the 10bp hairpin.

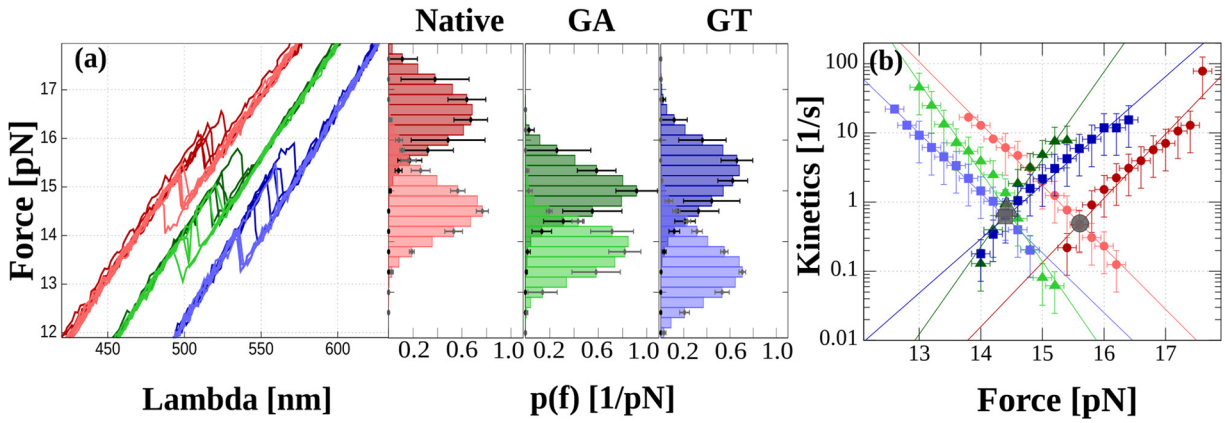

FIG. 3. 20bp hairpin pulling results. (a) Example of folding/unfolding pulling curves for native (red), G-A mismatch (green), and G-T mismatch (blue) 20bp hairpins. (b) Histograms of unfolding (dark colors) and folding forces (light colors). (c) Average kinetic rate as a function of the applied force. The black symbols indicate the coexistence force. Color code as in (a).

TABLE II. 20bp results. Parameters obtained from the pulling experiments for the 20 bp hairpins using the BE model and the theoretical ones obtained from the nearest-neighbor model.[3]

Hairpin	F_c (pN)	x_{NU} (nm)	$x_{N\to TS}$ (nm)	$x_{TS\to U}$ (nm)	ΔG^0_{NU} (k_BT)
20bp native	15.6 ± 0.2	17.7 ± 0.8	9.3 ± 0.4	8.4 ± 0.5	52 ± 3
Theor. native	16.0	18.2	/	/	54.0
20bp GA	14.4 ± 0.2	21.1 ± 3.0	10.3 ± 2.0	11.0 ± 1.2	48 ± 3
Theor. GA	14.6	17.9	/	/	48.0
20bp GT	14.4 ± 0.2	16.9 ± 1.2	8.3 ± 0.9	8.7 ± 0.3	48 ± 3
Theor. GT	14.5	17.9	/	/	47.4

This was achieved by fixing the center of mass of the first base-pair at one end of the dsDNA handles and by moving at constant velocity the center of mass of the first base-pair at the opposite end of the other handle. In this way, the opening λ between the two opposite ends of the dsDNA handles is linearly increasing with time from the zero-force value λ_0 = 23.0 nm with the hairpin in the folded state. For a pulling velocity in the range of a few cm/s, this translates into a similarly linear opening of the hairpin, as measured by looking at the relative distance between the sugar C1′ and the backbone P atoms of the first base pair (namely, the GC pair directly linked to the two dsDNA handles). The molecular extension has been chosen as the natural reaction coordinate to directly compare simulations and experiments, since the experiments allow us to measure, almost directly, the molecular extension. This choice is justified by the relative simplicity of the hairpin, as compared to complex molecules such as proteins, and the particular direction of the pulling protocol, different from the one used in DNA overstretching.[49] Unfolding of DNA hairpins occurs sequentially starting from the stem along the secondary structure of the hairpin. These considerations allow us to avoid the complexities of a multi-dimension FEL, for example, used in proteins.[50]

Figure 4 shows the result of these simulations. The simulated force-pulling experiments are followed up to the complete opening of the hairpin, over trajectories of a typical duration of ~ 50 ns. An example of the results is shown in Fig. 4(a), where the relative distance ("opening") between the C1′ atoms of each base pair in the hairpin is shown as a function of the simulation time (bp are numbered from 1, next to the loop, to 10, next to the dsDNA handles, see the inset). A first observation that clearly emerges from such a plot is that the unfolding of the hairpin does not seem to proceed by an ordered and progressive snapping of each base pair in sequence but rather follows a kind of collective process in which groups of bp open up simultaneously, e.g., at times ~17 and ~43 ns. Furthermore, the outermost bp (i.e., bp 10 in Fig. 4) seems to be already opened from the beginning of the simulation, and the second one follows almost immediately, after just a few ns. This observation may have interesting consequences to be discussed in the foregoing.

To bypass at least, in part, the time scale limitations of MD, we performed a second set of simulations by picking a few "interesting" configurations from the trajectory shown in Fig. 4(a), at times $t \simeq$ 7.5 ns, 18 ns, 22 ns, 28 ns, 35 ns, and 45 ns, corresponding to a relative opening between the opposite ends of the dsDNA handles of $\lambda \simeq$ 23.6 nm, 26.1 nm, 26.4 nm, 27.6 nm, 29.0 nm, and 31.1 nm. Each of these configurations was then run in a 100-ns MD simulation at constant-{NVT} with the fixed-λ external constraint (SHAKE–LINCS algorithms[41,51]). The hairpin equilibrium dynamics in such conditions may be seen as an approximation to a quasi-reversible pulling experiment but on the much faster MD time scale.

Figure 4(b) shows the equilibrium probability distributions of the C1′–C1′ distances for each bp of the hairpin, with color codes corresponding to those of Fig. 4(a). The four panels correspond to four progressive opening values, $\Delta\lambda = \lambda - \lambda_0$ = 0 nm, 0.6 nm, 4.4 nm, and 8 nm. It may be noted that, at zero opening (i.e., zero average external force), the equilibrium distribution confirms the above observation that the first base pair is constantly opened up, with a C1′–C1′ distance of about 1.9 nm. At $\Delta\lambda$ = 0.6 nm [corresponding to about t = 7.5 ns in Fig. 4(a)], the first two bp are spread open and the third one is just broadening its equilibrium width. At $\Delta\lambda$ = 4.4 nm (corresponding to $t \simeq$ 28 ns), the outermost six bp are widely opened, while the four inner ones are still closed at their equilibrium C1′–C1′ of 1.02 nm. Eventually, at $\Delta\lambda$ = 8 nm (corresponding to $t \simeq$ 45 ns), two more bp start opening and only the two bp closer to the hairpin loop are still in the closed state. Notably, at openings larger than about 3–4 nm, most base pairs display a doubly peaked distribution, very likely indicative of the rotational flipping in-and-out of these bases about the backbone and roughly parallel to the main hairpin axis.

In a last set of equilibrium MD simulations, we wanted to test the excitation dynamics of the hairpin. These simulations were run for 100 ns at constant-{NVT}, for all the values of fixed $\Delta\lambda$ above, by increasing the temperature of the simulation in steps of 10 K above room temperature. In Fig. 4(c), we present a subset of the results, namely, the data for one particular value of the opening, $\Delta\lambda$ = 4.4 nm, and for three temperatures T = 300 K, 320 K, and 340 K. At such opening, each 20 K increase in temperature corresponds to an applied force $\Delta f \simeq$ 18.5 pN, which is a value comparable to the experimental coexistence force f_c. Therefore, by running MD at 320 K and 340 K under fixed opening, we are simulating the effect of injecting once/twice an amount of energy $\Delta f \cdot \Delta\lambda$: for a fixed $\Delta\lambda$, this would correspond to proportionally increasing the effective stiffness of the optical trap. Figure 4(c) shows the probability distributions for bp 10–4, the innermost 3 bp remaining closed at any temperature; the traces in color correspond to T = 300 K (blue), 320 K (black), and 340 K (red). It is noted that, at room temperature, the energy injected to keep the hairpin at the opening of $\Delta\lambda$ = 4.4 nm is unevenly distributed among the outermost bp (6–10, with the five

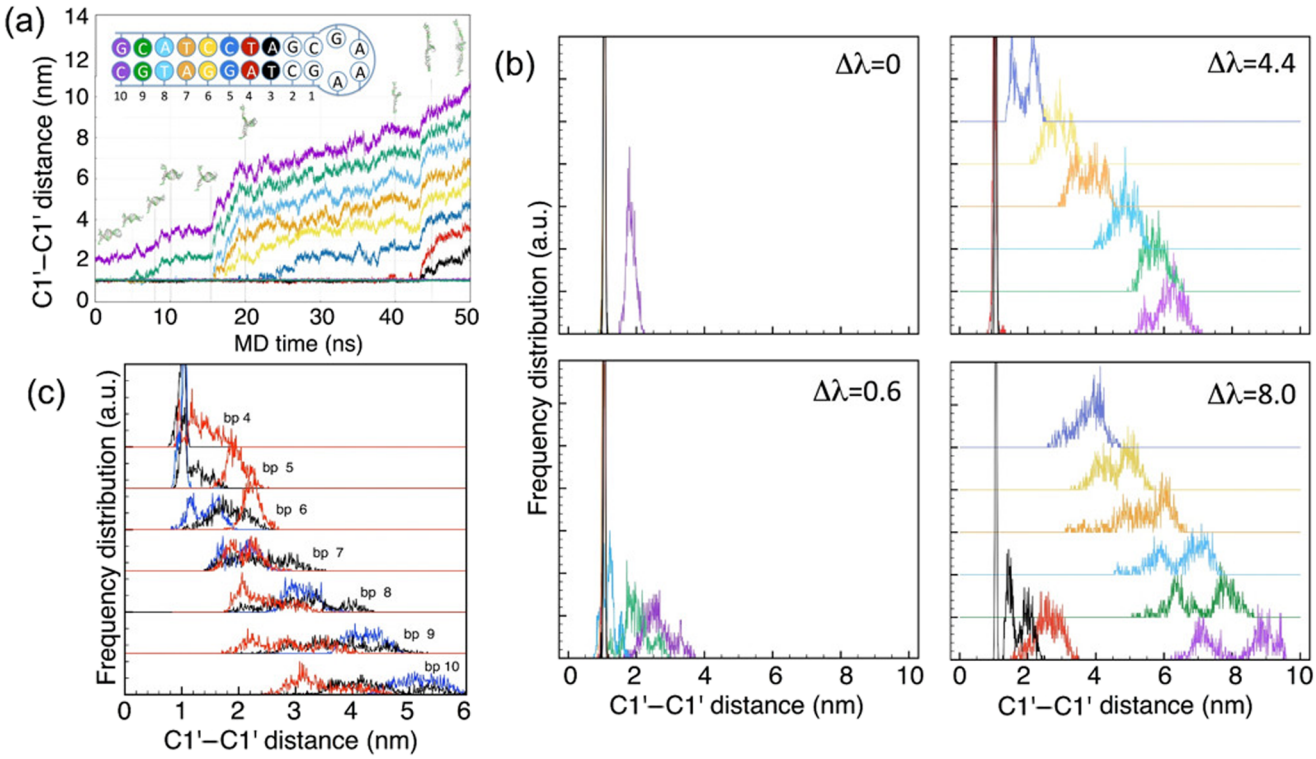

FIG. 4. MD simulations. (a) Constant pulling speed (about 10^6–10^7 times larger than in the experiments) and T = 300 K for the 10bp hairpin with the native sequence (shown in the inset with bp numbering and color codes). The 50-ns long time traces, starting from the folded state and going to the fully unfolded, display the relative distance between the sugar C1′ atoms of each base pair, as indicated in the legend (the bp number 10 being the one close to the dsDNA handles and the bp number 1 being the one adjacent to the loop). Above the plots, schematic snapshots give a visual indication of the average molecular configuration of the hairpin at approximately the time corresponding on the x-axis. (b) Equilibrium probability histograms for the C1′–C1′ distance of each bp in the native hairpin from 100-ns long MD {*NVT*} trajectories at $\Delta\lambda$ = 0 nm, 0.6 nm, 4.4 nm, and 8 nm. The histograms are colored according to the bp scheme of panel (a); data for the two larger $\Delta\lambda$ are shifted upwards on the y-axis for better clarity.(c) Equilibrium histograms for the C1′–C1′ distance of each bp in the native hairpin [numbered according to the inset scheme in panel (a)], from 100-ns long MD {*NVT*} trajectories at fixed $\Delta\lambda$ = 4.4 nm, and different temperatures: T = 300 K (blue), 320 K (black), and 340 K (red).

only slightly excited), which display average amplitudes decreasing toward the loop end; the width of the distribution is nearly double for the outermost bp 10, compared to the other ones. As the injected energy (i.e., temperature) is increased, the distributions tend to become more even (centroid of the distribution decreasing for bp 8–10 and increasing for bp 4–7), while, at the same time, each distribution covers a very broad range of bp opening, spread over about 2 nm for the outermost bp. We interpret these results as the effect of increased cooperativity in the unfolding transition at high values of force: while at low forces, the bp tend to open individually or in small batches, at high applied forces, unfolding appears to occur by a simultaneous opening of the entire hairpin.

DISCUSSION AND CONCLUSIONS

The ability to detect point defects along the sequence of a DNA molecule is a relevant problem, both for molecular biology studies of DNA replication and damage repair and for the many technological applications exploiting base-pair complementarity of nucleic acids (e.g., PCR and DNA self-assembly). However, differences in base pairing between the native, Watson–Crick A-T and G-C purine–pyrimidine pairs, and the defective ones, typically including mismatches (MMs), are very subtle and escape a direct experimental determination. The effect of a MM in a random position of a DNA sequence may reveal itself as a small local difference in free energy, which, however, shows up only when the two DNA strands are split apart, e.g., during replication, or as a small variation in the elastic and mechanical properties of the molecule to an applied stress, e.g., by a repair enzyme.

In this work, we used single-molecule force spectroscopy with LOT to demonstrate the ability of this experimental method to detect the small free-energy and force differences associated with a single, isolated MM in a DNA sequence. As a test system, we adopted a short self-complementary hairpin undergoing a reversible folding/unfolding transition with the aim of extracting information about the differences induced in this dynamical transition by the presence of a G-A or G-T mismatch, inserted in the middle of the hairpin. This same system was used in a recent work[32] in which longer hairpin constructs including pairs of MM were

used. With respect to that work, here, we tested the lower limits of the technique to detect a single defect in the shortest possible sequence. To this end, we used hairpins of length 10 and 20 bp in hopping and pulling experiments, respectively. Both methods showed pros and cons, namely, (a) the hopping method is more adapted to the shorter 10bp hairpins, since the folding/unfolding rate is exponentially larger; therefore, a large number of folding/unfolding transitions can be observed in this case, with much better statistics. (b) The force-pulling method is more adapted to the longer 20bp hairpins, since the difference between the folding/unfolding force path is proportional to the hairpin length, and for the shorter ones, the two force branches are so close to be nearly indistinguishable.

In both sets of experiments, we could clearly demonstrate the detection of a single MM in the hairpin, both in the form of a lower free energy, ΔG_0, and a lower coexistence force, f_c (see Tables I–III). However, the difference in free energy between the hairpins with G-T and G-A mismatches obtained using both methods, pulling and hopping experiments, shows similar and compatible values (see Table IV). An improved estimate of the relative free-energy differences $\Delta\Delta G$ between the native and mismatched sequences for the 10bp hairpin can be obtained by subtracting the two independent values ΔG and ΔG_0 obtained from kinetics [Eq. (3)] and thermodynamics [Eq. (4)]. We obtain $\Delta\Delta G_{GA} = 4 \pm 2$ kcal/mol and $\Delta\Delta G_{GT} = 4.5 \pm 2$ kcal/mol.

As already noted, the absolute values of free-energy for the 10bp hairpin in Tables I and III appear to be lower (by ~15%) than the nearest-neighbor (NN) model prediction.[52] This agrees with the trend observed for the lower values obtained for f_c and x_{NU} as compared to the theoretical predictions (Table I). Yet, for the native 10bp hairpin, we find a value of ΔG_0 that falls closer to the unzipping prediction. The opposite situation is found for the 20bp native hairpin where the NN prediction works better than the unzipping prediction (Tables II and III). Overall this suggests that, for the 10bp and 20bp hairpins, the measured and predicted energy numbers agree within errors.

However, we cannot exclude the possibility that the apparently lower thermodynamic stability (and lower f_c and x_{NU}) of the 10bp hairpin arises from fraying effects. Note that the 10bp hairpin has only two GC bp at the beginning of the stem followed by two AT bp that render the fork less stable. MD simulations, reported in the Section Simulation results show that the first base-pair in the hairpin stem appears to be always opened, even at zero applied force, decreasing the folding free energy of the hairpin as observed. This same effect was observed also in the longer hairpins of the study by McCauley *et al.*[32] The MD simulations suggest that the first bp of the hairpin could be already open even before the hairpin unfolds. To test this possibility, we have compared the experimental results with the NN model ignoring the contribution of the first G-C pair in the 10bp hairpin (NN*). The new NN* energies show a lower value than the experimental ones for the 10bp case, making the experimental values fall in between the two predictions (NN and NN*). The energy numbers are (in kcal/mol) as follows:

- 10bp native 11.8(NN*) < 12.5 (exp) < 14.3 (NN),
- 10bp G-A 8.2(NN*) < 9.5 (exp) < 10.7 (NN), and
- 10bp G-T 7.9(NN*) < 9.5 (exp) < 10.4 (NN).

Fraying might be tested in future experiments and simulations as a possible explanation by studying 10bp hairpins with more stable stems. Overall, the results show the power of combining computer simulations and experiments to improve the models used to interpret the experimental data. Note that, for the 20bp, the NN values and the experimental ones are compatible (Table III); therefore, application of a NN correction in this case might be unnecessary. There are two possible explanations for such a difference. First, while the 10bp hairpin starts with two G-C bp at the beginning of the stem, the 20bp has seven G-C bp. Second, in the 10bp hairpin, the distance between the fork and the MM position (4–5bp) is well below the 10–11 nucleotides (a full turn of the double helix), which is generally considered as the limit for two defects to interact. For the 20bp hairpin, such a distance (9–10 nucleotides) is larger. Future studies might consider addressing the fraying problem in more detail.

In the Bell–Evans model, the folding/unfolding process is described by a thermally activated diffusive process across an energy barrier,[53] separating two independent conformations of the molecule. The combined Bell–Evans and HMM analysis of the hopping data for the 10bp defective hairpins did not show evidence of an intermediate state possibly caused by the mismatch (see Figs. 4 and 5 in the supplementary material). The same was found in preliminary hopping data for the 20bp defective hairpins. The MD simulations demonstrated a variable degree of cooperativity in the folding/unfolding transition of the 10bp native hairpin in that at lower forces, the hairpin appears to unfold in a sequential way, but with groups of bases opening up together, while at higher forces, the hairpin tends to open up in one collective snapping of the bonds

TABLE III. Folding free energies for the 10bp and 20bp DNA hairpins. Experimental data (second column) are compared with the estimates obtained from the nearest-neighbor (NN) model using the energies from SantaLucia[3] or from unzipping experiments.[35]

Hairpin	ΔG_0 (kcal/mol)	NN[3] (kcal/mol)	Unzipping[35] (kcal/mol)
10bp native	12.5 ± 2	14.3	12.0
10bp GA	9.5 ± 1	10.7	...
10bp GT	9.5 ± 1	10.4	...
20bp native	31.5 ± 1	32.0	29.5
20bp GA	28.5 ± 1	28.4	...
20bp GT	28 ± 1	28.1	...

TABLE IV. Folding free-energy differences $\Delta\Delta G_0$ between the native and mismatched sequences obtained from different experiments, compared with NN model predictions. $\Delta\Delta G_0$ is obtained from the results shown in Tables I–III.

Hairpin	$\Delta\Delta G_0$ (kcal/mol)	NN model (kcal/mol)
10bp GA	3 ± 3	3.6
20bp GA	3 ± 2	3.7
10bp GT	3 ± 3	3.9
20bp GT	3.5 ± 2	3.8

between bps. For a given displacement λ, a larger force translates into a stiffer optical trap, and such an increase in cooperativity with stiffer coupling is in agreement with a previous experimental study[54] and theoretical models.[55,56] The transition from an additive to a collective unfolding may also be interpreted in terms of an increasing "friction" effect that builds up between the closed bps, which must overcome a twist elastic barrier, at the same time, as the chemical bond-breaking barrier;[57] however, in the present case, this effect would be driven by a variable force, rather than by variation in the polymer physical length.

In conclusion, the results and potential implications of this study can be summarized by the following findings:

1. Single-molecule force spectroscopy with LOT permits us to identify the presence of a single mismatched base-pair in short 10–20 bp DNA hairpins. The mismatch decreases the thermodynamic stability of the hairpin (by lowering its free-energy of formation and coexistence force). It also speeds up the kinetics of folding of the hairpin to a larger extent by lowering the height of the barrier.
2. Passive hopping experiments allow us to detect a single mismatch in 10bp hairpins, while pulling experiments produce a better signal in longer sequences (20bp).
3. The folding/unfolding transition in the 10bp and 20bp defective hairpins is well described by a two-state model, without evidence for intermediate states. This result is based on the analysis of hopping experiments and a hidden-Markov model.
4. MD simulations of the hairpin unfolding transition under external force support this view and provide important clues for the analysis of experimental data; simulations also suggest a variable degree of cooperativity in base-pair opening during the forced unfolding.

The folding/unfolding transition in short hairpins is therefore a relevant test bed for studying defects in DNA. Further work should concentrate in refining the experimental setup, in order to arrive at a better quantitative characterization of point defects, and move toward the study of the role of signalization and repair proteins in defect dynamics. MD simulations can play a relevant role in assisting and guiding the experimental analysis.

SUPPLEMENTARY MATERIAL

See the supplementary material for additional information on DNA hairpin synthesis, free energy difference between folded and unfolded states, hairpin free energy landscape, and a detailed analysis of the hopping/pulling experiments.

ACKNOWLEDGMENTS

F.L. is thankful to the Doctoral School SPI-079 and the IEMN Excelsior Labex Project for additional financial support. He is also thankful to the Small Systems Lab for additional financial support and for their kind hospitality during his extended stay in Barcelona. We acknowledge partial funding from the SIRIC OncoLille under project "ModCel." Computer resources provided by the CINES and IDRIS French Supercomputing Centres, under Grant Nos. a0020707225 and x2016/077225, and by generous extensions thereof. F.R., X.V.-G., and I.P. acknowledge support from Catalan ICREA Academia Prizes 2013 and 2018 and the Spanish Research Council (Grant No. FIS2016-80458-P).

The authors declare no competing interests.

REFERENCES

[1] P. Modrich, "DNA mismatch correction," Annu. Rev. Biochem. **56**, 435–466 (1987).
[2] A. Tikhomirova, I. V. Beletskaya, and T. V. Chalikian, "Stability of DNA duplexes containing GG, CC, AA, and TT mismatches," Biochemistry **45**, 10563–10571 (2006).
[3] N. Peyret, P. A. Seneviratne, H. Allawi, and J. SantaLucia, "Nearest-neighbor thermodynamics and NMR of DNA sequences with internal AA, CC, GG, and TT mismatches," Biochemistry **38**, 3468–3477 (1999).
[4] G. Rossetti, P. D. Dans, I. Gomez-Pinto, I. Ivani, C. Gonzalez, and M. Orozco, "The structural impact of DNA mismatches," Nucl. Acids Res. **43**, 4309–4321 (2015).
[5] M. F. Goodman, S. Creighton, L. B. Bloom, and J. Petruska, "Biochemical basis of DNA replication fidelity," Crit. Rev. Biochem. Mol. Biol. **28**, 83–126 (1993).
[6] J. Wildenberg and M. Meselson, "Mismatch repair in heteroduplex DNA," Proc. Natl. Acad. Sci. U. S. A. **72**, 2202–2206 (1975).
[7] C. Kunz, Y. Saito, and P. Schär, "DNA repair in mammalian cells," Cell. Mol. Life Sci. **66**, 1021–1038 (2009).
[8] P. Modrich, "Mechanisms in eukaryotic mismatch repair," J. Biol. Chem. **281**, 30305–30309 (2006).
[9] R. D. Kolodner, "Mismatch repair: Mechanisms and relationship to cancer susceptibility," Trends Biochem. Sci. **20**, 397–401 (1995).
[10] S. S. David, V. L. O'Shea, and S. Kundu, "Base-excision repair of oxidative DNA damage," Nature **447**, 941–950 (2007).
[11] A. Meyerhans and J.-P. Vartanian, "The fidelity of cellular and viral polymerases and its manipulation," in *Origin and Evolution of Viruses*, edited by E. Domingo, R. G. Webster, and J. F. Holland (Academic Press, New York, 1999), Chap. 5.
[12] P. M. Lizardi, X. Huang, Z. Zhu, P. Bray-Ward, D. C. Thomas, and D. C. Ward, "Mutation detection and single-molecule counting using isothermal rolling-circle amplification," Nat. Gen. **19**, 225–232 (1998).
[13] P. Hardenbol, J. Banér, M. Jain, M. Nilsson, E. A. Namsaraev, G. A. Karlin-Neumann, H. Fakhrai-Rad, M. Ronaghi, T. D. Willis, and U. Landegren, *et al.* "Multiplexed genotyping with sequence-tagged molecular inversion probes," Nat. Biotechnol. **21**, 673–678 (2003).
[14] Q. Xu, S. Q. Huang, F. Ma, B. Tang, and C. Y. Zhang, "Controllable mismatched ligation for bioluminescence screening of known and unknown mutations," Anal. Chem. **88**, 2431–2439 (2016).
[15] F. M. De La Vega, K. D. Lazaruk, M. D. Rhodes, and M. H. Wenz, "Assessment of two flexible and compatible SNP genotyping platforms: TaqMan® SNP genotyping assays and the SNPlex™ genotyping system," Mutat. Res., Fundam. Mol. Mech. Mutagen. **573**, 111–135 (2005).
[16] S. Tyagi and F. R. Kramer, "Molecular beacons: Probes that fluoresce upon hybridization," Nat. Biotechnol. **14**, 303–308 (1996).
[17] R. Wagner, P. Debble, and M. Radman, "Mutation detection using immobilized mismatch binding protein (MutS)," Nucl. Acids Res. **23**, 3944–3948 (1995).
[18] B. J. Till, C. Burtner, L. Comai, and S. Henikoff, "Mismatch cleavage by single-strand specific nucleases," Nucl. Acids Res. **32**, 2632–2641 (2004).
[19] D. J. Patel, S. A. Kozlowski, L. A. Marky, J. A. Rice, C. Broka, J. Dallas, K. Itakura, and K. Breslauer, "Structure, dynamics, and energetics of deoxyguanosine·thymidine wobble base pair formation in the self-complementary d(CGTGAATTCGCG) duplex in solution," Biochemistry **21**, 437–444 (1982).
[20] D. J. Patel, A. Pardi, and K. Itakura, "DNA conformation, dynamics, and interactions in solution," Science **216**, 581–590 (1982).
[21] D. Rabinovich, T. Haran, M. Eisenstein, and Z. Shakked, "Structures of the mismatched duplex d(GGGTGCCC) and one of its Watson-Crick analogues d(GGGCGCCC)," J. Mol. Biol. **200**, 151–161 (1988).

[22]T. Brown, O. Kennard, G. Kneale, and D. Rabinovich, "High-resolution structure of a DNA helix containing mismatched base pairs," Nature **315**, 604–606 (1985).
[23]J. I. Friedman and J. T. Stivers, "Detection of damaged DNA bases by DNA glycosylase enzymes," Biochemistry **49**, 4957–4967 (2010).
[24]Y. Qi, M. C. Spong, K. Nam, A. Banerjee, S. Jiralerspong, M. Karplus, and G. L. Verdine, "Encounter and extrusion of an intrahelical lesion by a DNA repair enzyme," Nature **462**, 762–766 (2009).
[25]Y. Suzuki and O. K. Dudko, "Single-molecule rupture dynamics on multidimensional landscapes," Phys. Rev. Lett. **104**, 048101 (2010).
[26]C. Bustamante, J. F. Marko, E. D. Siggia, and S. Smith, "Entropic elasticity of lambda-phage DNA," Science **265**, 1599–1601 (1994).
[27]S. B. Smith, Y. Cui, and C. Bustamante, "Overstretching B-DNA: The elastic response of individual double-stranded and single-stranded DNA molecules," Science **271**, 795–799 (1996).
[28]C. Bouchiat, M. Wang, J.-f. Allemand, T. Strick, S. Block, and V. Croquette, "Estimating the persistence length of a worm-like chain molecule from force-extension measurements," Biophys. J. **76**, 409–413 (1999).
[29]F. Ritort, "Single-molecule experiments in biological physics: Methods and applications," J. Phys. Condens. Matter **18**, R531–R583 (2006).
[30]A. Alemany and F. Ritort, "Determination of the elastic properties of short ssDNA molecules by mechanically folding and unfolding DNA hairpins," Biopolymers **101**, 1193–1199 (2014).
[31]A. Alemany and F. Ritort, "Force-dependent folding and unfolding kinetics in DNA hairpins reveals transition-state displacements along a single pathway," J. Phys. Chem. Lett. **8**, 895–900 (2017).
[32]M. J. McCauley, L. Furman, C. A. Dietrich, I. Rouzina, M. E. Nunez, and M. C. Williams, "Quantifying the stability of oxidatively damaged DNA by single-molecule DNA stretching," Nucl. Acids Res. **46**, 4033–4043 (2018).
[33]B. D. Sattin, A. E. Pelling, and M. C. Goh, "DNA base pair resolution by single molecule force spectroscopy," Nucl. Acids Res. **32**, 4876–4883 (2004).
[34]W. Liu, Y. Guo, K. Wang, X. Zhou, Y. Wang, J. Lü, Z. Shao, J. Hu, D. M. Czajkowsky, and B. Li, "Atomic force microscopy-based single-molecule force spectroscopy detects DNA base mismatches," Nanoscale **11**, 17206–17210 (2019).
[35]J. M. Huguet, C. V. Bizarro, N. Forns, S. B. Smith, C. Bustamante, and F. Ritort, "Single-molecule derivation of salt dependent base-pair free energies in DNA," Proc. Natl. Acad. Sci. U. S. A. **107**, 15431–15436 (2010).
[36]M. Manosas, D. Collin, and F. Ritort, "Force-dependent fragility in RNA hairpins," Phys. Rev. Lett. **96**, 218301 (2006).
[37]E. Evans and K. Ritchie, "Dynamic strength of molecular adhesion bonds," Biophys. J. **72**, 1541–1555 (1997).
[38]E. Evans, "Probing the relation between force-lifetime-and chemistry in single molecular bonds," Annu. Rev. Biophys. Biomol. Struct. **30**, 105–128 (2001).
[39]A. Mossa, J. M. Huguet, and F. Ritort, "Investigating the thermodynamics of small biosystems with optical tweezers," Physica E **42**, 666–671 (2010).
[40]H. Berendsen, D. van der Spoel, and R. van Drunen, "GROMACS: A message-passing parallel molecular dynamics implementation," Comput. Phys. Commun. **91**, 43–56 (1995).
[41]E. Lindahl, B. Hess, and D. van der Spoel, "GROMACS 3.0: A package for molecular simulation and trajectory analysis," J. Mol. Model. **7**, 306–317 (2001).
[42]B. E. K. Snodin, F. Randisi, M. Mosayebi *et al.*, "Introducing improved structural properties and salt dependence into a coarse-grained model of DNA," J. Chem. Phys. **142**, 234901 (2015).
[43]C. Hyeon and D. Thirumalai, "Capturing the essence of folding and functions of biomolecules using coarse-grained models," Nat. Commun. **2**, 487 (2011).
[44]O. Henrich, Y. G. Fosado, T. Curk *et al.*, "Coarse-grained simulation of DNA using LAMMPS: An implementation of the OXDNA model and its application," Eur. Phys. J. E **41**, 57 (2018).
[45]T. E. Ouldridge, A. A. Louis, and J. P. K. Doye, "Structural, mechanical, and thermodynamic properties of a coarse-grained DNA model," J. Chem. Phys. **134**, 085101 (2011).
[46]N. Forns, S. de Lorenzo, M. Manosas, K. Hayashi, J. M. Huguet, and F. Ritort, "Improving signal/noise resolution in single-molecule experiments using molecular constructs with short handles," Biophys. J. **100**, 1765–1774 (2011).
[47]G. I. Bell, "Models for the specific adhesion of cells to cells," Science **200**, 618–627 (1978).
[48]M. Zuker, "Mfold web server for nucleic acid folding and hybridization prediction," Nucl. Acids Res. **31**, 3406–3415 (2003).
[49]A. Garai, S. Mogurampelly, S. Bag, and P. K. Maiti, "Overstretching of B-DNA with various pulling protocols: Appearance of structural polymorphism and S-DNA," J. Chem. Phys. **147**, 225102 (2017).
[50]A. K. Sahoo, B. Bagchi, and P. K. Maiti, "Unfolding dynamics of ubiquitin from constant force MD simulation: Entropy-enthalpy interplay shapes the free-energy landscape," J. Phys. Chem. B **123**, 1228–1236 (2019).
[51]B. J. Berne, G. Ciccotti, and D. F. Coker, *Classical and Quantum Dynamics in Condensed Phase Simulations* (World Scientific Publishing Co. Pte. Ltd., 1998).
[52]S. Cocco, J. F. Marko, and R. Monasson, "Slow nucleic acid unzipping kinetics from sequence-defined barriers," Eur. Phys. J. E **10**, 153–161 (2003).
[53]P. Hänggi, P. Talkner, and M. Borkovec, "Reaction-rate theory: Fifty years after Kramers," Rev. Mod. Phys. **62**, 251 (1990).
[54]J. M. Huguet, N. Forns, and F. Ritort, "Statistical properties of metastable intermediates in DNA unzipping," Phys. Rev. Lett. **103**, 248106 (2009).
[55]F. Manca, S. Giordano, P. Palla, F. Cleri, and L. Colombo, "Monte Carlo simulations of single polymer force-extension relations," J. Phys.: Conf. Ser. **383**, 012016 (2012).
[56]F. Manca, S. Giordano, P. Palla, F. Cleri, and L. Colombo, "Two-state theory of single-molecule stretching experiments," Phys. Rev. E **87**, 032705 (2013).
[57]J. Hooyberghs, P. V. Hummelen, and E. Carlon, "The effects of mismatches on hybridization in DNA microarrays: Determination of nearest neighbor parameters," Nucl. Acids Res. **37**, e37 (2009).